arXiv:1512.05084v1 [cond-mat.mtrl-sci] 16 Dec 2015

First-Principles Computation of G-Factors in Bi and Bi_2Se_3

Zhida Song,[1] S. M. Nie,[1] Zhong Fang,[1,2] and Xi Dai[1,2,*]

[1] *Beijing National Laboratory for Condensed Matter Physics, and Institute of Physics, Chinese Academy of Sciences, Beijing 100190, China*

[2] *Collaborative Innovation Center of Quantum Matter, Beijing, 100084, China*

(Dated: December 17, 2015)

Abstract

In this paper, we propose a first principles computation method for g-factor tensor, which not only gives comparable results with experiments but also establishes a clear physical picture of Zeeman effect in materials. In our method, the Hilbert space of the electronic states is treated as a direct product of "inner" space and "orbital" space, which are spanned by Bloch wave functions and envelope functions respectively. Correspondingly, vector-potential is divided into a periodic part acting only in inner space and a non-periodic part acting only in orbital space. With the above flamework we define the g-factors as coupling coefficients between inner space and magnetic field. By the method we developed, we have further computed the g-factors of bismuth and Bi_2Se_3 and got satisfactory results, which are in good agreement with the experimental data.

I. INTRODUCTION

The theory of g-factor in materials has been an old topic in condensed matter physics. The widely used theory has been developed by Luttinger[1] and Cohen[2] in 1950s, in which the extra Zeeman term comes from the commutator of $\hat{\mathbf{p}} + \mathbf{A}$ in second order perturbation approach. That the extra term is propotional to the orbital magnetic momentum of Bloch state instead of spin momentum reveals a good physics picture of Zeeman splitting in materials. This physical picture has been re-clarified by Chang and Niu[3,4] in 1996 as the effect of self-rotating of semi-classical wave packet. Niu's theory is closely related to the modern theory of polarization[5–7] since both of them can be ascribed to geometry (Berry) phase effects in the adiabatic evolution process of Bloch states driven by external electromagnetic fields. Detailed description of Berry phase and its relation to orbital magnetic momentum could be found in review [8] and [9]. Although the formula and physical meaning of Zeeman splitting in materials have been known for a long time, first principles calculations are lacking seriously, which comes with a lot of ambiguities and arguments on g-factor's values and mechanisms in some materials. For example, there are a lot of different suggestions on the reason of large g-factors in bismuth and Bi_2Se_3.[10–12] We expect to solve this by first principles calculations.

In this paper, we firstly supply an alternative derivation of Zeeman term and then establish a first principles method to calculate the g-factor. In our derivation, the Hilbert space is decomposed as direct product of an "inner" space spanned by some fast varing Bloch states and an "orbital" space spanned by slowly varing envelope functions. We take the Coulomb gauge for vector potential, i.e. $\mathbf{A} = \frac{1}{2}\mathbf{B} \times \mathbf{r}$, and divide the vector potential into a translational invariant (periodic) part and a translational variant (non-periodic) part. The periodic component keeps the band structure and couples with the inner space by shifting the levels of Bloch states due to their total magnetic momentums, while the non-periodic component breaks band structure and drives the electrons to form Landau levels. Therefore we define g-factors as the coupling coefficients between the inner space and magnetic field. According to this definition, we have built a first principles computation method and realized it based on the Vienna ab-initio simulation package (VASP). By the code, the g-factors of bismuth and Bi_2Se_3 have been computed first-principlely. Comparable results with experimental data have been got. We show that the strong anisotropy of g-factors in bismuth

is a direct consequence of group representation. And the large values of g-factors in both bismuth and Bi_2Se_3 can be ascribed to the large Dirac velocities or small gaps.

The paper is organized as follows. In section II, the formula is derived and the physical picture is clarified. Then the first principles computation method is established. In section III, g-factors of bismuth and Bi_2Se_3 are computed and discussed. In section IV, a brief summary is supplied.

II. METHOD

Single particle hamiltonian of electrons in a crystal can be written as:

$$\begin{aligned} H = & \frac{(\hat{\mathbf{p}} + e\mathbf{A})^2}{2m} + V_0(\mathbf{r}) + V(\mathbf{r}) \\ & + \frac{\hbar}{4m_0^2c^2}(\hat{\mathbf{p}} + e\mathbf{A}) \cdot \boldsymbol{\sigma} \times V_0(\mathbf{r}) + \mu_B \frac{g_0}{2} \boldsymbol{\sigma} \cdot \mathbf{B} \end{aligned} \tag{1}$$

where $\hat{\mathbf{p}}$ is canonical momentum operator $-i\hbar\nabla$, V_0 is the crystal periodic potential, $\boldsymbol{\sigma}$ is pauli matrices, V is external scaler potential, $\mathbf{B}$ is external magnetic field, and $\mathbf{A}$ is vector potential. For numerical purpuse, we choose Coulomb gauge for vector potential: $\mathbf{A} = \frac{1}{2}\mathbf{B} \times \mathbf{r}$. The fourth term in Eq. (1) is spin-orbit coupling (SOC). The last term is the bare Zeeman effect with free electron's g-factor g_0. In this paper, we only take into account weak external fields, hence SOC comes from V has been savely neglected in Eq. (1).

Because external fields usually break translational symmetry, eigenstates of the above hamiltonian can not hold Bloch theorem. However, we can handle this problem by envelope functions method in which wave function is decomposed as a set of products of Bloch wave functions and envelope functions. Although envelope functions are nothing new in semiconductor physics, we give an alternative treatment of vector potential's matrix elements which will give a better understanding of Zeeman effects in crystals.

A. Orbital Space and Inner Space

In semiconductors or insulators, the effective theory is usually a k·p model expanded on the Bloch wave functions at a high symmetry k point, which we denote as $\mathbf{k}_0$. Here we keep the same spirit, thus we construct the following basis set with index $(n, \mathbf{k})$:

$$\phi_{n\mathbf{k}}(\mathbf{r}) = e^{i\Delta\mathbf{k}\cdot\mathbf{r}}\phi_{n\mathbf{k}_0}(\mathbf{r}) = e^{i\mathbf{k}\cdot\mathbf{r}}u_{n\mathbf{k}_0}(\mathbf{r}) \tag{2}$$

$\phi_{n\mathbf{k}_0}(\mathbf{r})$ is chosen as the n-th Bloch wave function at $\mathbf{k}_0$, $u_{n\mathbf{k}_0}(\mathbf{r})$ is the periodic part of $\phi_{n\mathbf{k}_0}(\mathbf{r})$. Notice that $\phi_{n\mathbf{k}\neq\mathbf{k}_0}$ is not a Bloch state but only a constructed basis for converniance. Now $\mathbf{k}_0$ is chosen as the origin of momentum and $\Delta\mathbf{k} = \mathbf{k} - \mathbf{k}_0$ measures momentums from it. Thus, we define $\mathbf{k}$ in a Brillouin zone (BZ) centered at $\mathbf{k}_0$ as shown in Fig. 1. We find the basis set defined in Eq. (2) is orthogonal with each other, and is complete if n takes value of all bands. The orthogonality is apparent: bases at different $\mathbf{k}$ are orthogonal with each other because of momentum conservation and the orthogonality of the bases at same wave vector comes from the orthogonality of $u_{n\mathbf{k}_0}$. The completeness is also easy to understand. Since $\{u_{n\mathbf{k}_0}\}$ serves as a complete basis set for periodic functions, any Bloch wave functions $e^{i\mathbf{k}\cdot\mathbf{r}}u_{n\mathbf{k}}$ can be expanded by $\phi_{n\mathbf{k}} = e^{i\mathbf{k}\cdot\mathbf{r}}u_{n\mathbf{k}_0}$, which indicates the completeness. A detailed proof of orthogonality and completeness can be found in Luttinger and Kohn's early work[13].

Therefore, we can expand the eigen wave function of Eq. (1) on the basis set:

$$\begin{aligned}\Psi(\mathbf{r}) &= \sum_{n\mathbf{k}} w_n(\mathbf{k})\phi_{n\mathbf{k}}(\mathbf{r}) \\ &= \sum_{n} \psi_n(\mathbf{r})\phi_{n\mathbf{k}_0}(\mathbf{r}) \end{aligned} \tag{3}$$

$$\psi_n \equiv \sum_{\mathbf{k}} w_n(\mathbf{k})e^{i\Delta\mathbf{k}\cdot\mathbf{r}} \tag{4}$$

where ψ_n is defined as envelope functions. It is vital to recognize Fourier components of ψ_n and $\phi_{n\mathbf{k}_0}$ belong to two independent subspaces : ψ_n is spanned by plane waves $e^{i\Delta\mathbf{k}\cdot\mathbf{r}}$ where $\Delta\mathbf{k}$ takes value in BZ (as shown in Fig. 1), while $\phi_{n\mathbf{k}_0}$ is spanned by $e^{i(\mathbf{k}_0+\mathbf{G})\cdot\mathbf{r}}$, where $\mathbf{G}$ is reciprocal vector. Indeed, in Fourier representation the bases defined in Eq. (2) are direct products of bases in the two subspace:

$$\langle\mathbf{k}' + \mathbf{G}'|\phi_{n\mathbf{k}}\rangle = \langle\Delta\mathbf{k}'|\Delta\mathbf{k}\rangle \otimes \langle\mathbf{k}_0 + \mathbf{G}'|\phi_{n\mathbf{k}_0}\rangle \tag{5}$$

We call the space spanned by $e^{i(\mathbf{k}_0+\mathbf{G})\cdot\mathbf{r}}$ the inner space and call the space spanned by $e^{i\Delta\mathbf{k}\cdot\mathbf{r}}$ the orbital space. By this definition, envelope functions ψ_n belong to orbital space while Bloch wave functions $\phi_{n\mathbf{k}_0}$ belong to inner space. Then we find the wave function can be decomposed as direct products of envelope functions and Bloch wave functions:

$$\begin{aligned}\langle\mathbf{k}' + \mathbf{G}'|\Psi\rangle &= \sum_{n\mathbf{k}} w_n(\mathbf{k})\langle\mathbf{k}' + \mathbf{G}'|\phi_{n\mathbf{k}}\rangle \\ &= \sum_{n}\langle\Delta\mathbf{k}'|\psi_n\rangle \otimes \langle\mathbf{k}_0 + \mathbf{G}|\phi_{n\mathbf{k}_0}\rangle \end{aligned} \tag{6}$$

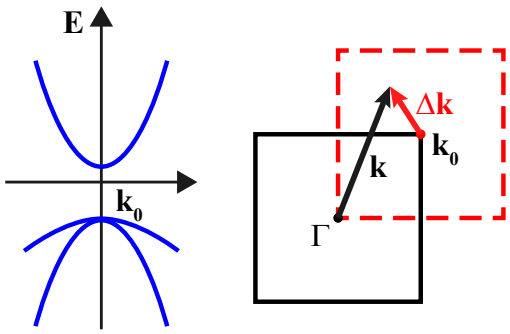

FIG. 1: Range of wave vector of basis $\phi_{n\mathbf{k}}$. $\mathbf{k}$ takes value in the BZ plotted with red (dashed) lines which is shifted from the first BZ (potted with black (solid) lines) by a vector $\mathbf{k}_0$. $\mathbf{k}_0$ is usually chosen as the bands minimum point or maximum point.

i.e.:

$$|\Psi\rangle = \sum_n |\psi_n\rangle \otimes |\phi_{n\mathbf{k}_0}\rangle \tag{7}$$

We note that the expansion in Eq. (4) or Eq. (7) is rigorous due to the completeness of basis set. Approximations can only come from the cutoff of bands index n. As external fields under consideration are weak, the wave functions near fermi level should not alter too much from the original Bloch wave functions near fermi level. Therefore it is usually enough to keep the degenerate or quasi-degenerate bands near fermi level to capture the low energy physics. For the purpose of a complete analysis, we keep all the bands for now.

The direct product structure also reveals a reasonable physical picture. In low energy scale, deformations of wave functions are described by a few smooth envelope functions ψ_n. ψ_n varies so slowly that we should measure it on a mesoscopic scale on which we are blind to see the microcosmic fast oscillations of Bloch wave functions. Namely, the detailed information of Bloch wave functions is hidden in such mesoscopic physics. The only information left for us is that at each position (in real space or momentum space) the wave function is attached with a set of Bloch states described by an inner space vector, which is very similar with the case of spin in schrödinger's equation. This is why we call the space spanned by $\phi_{n\mathbf{k}_0}$ (or $e^{i(\mathbf{k}_0+\mathbf{G})\cdot\mathbf{r}}$) the inner space.

Now we go further to decompose operators into direct product form. Due to distributive

property of derivation, momentum operator is decomposed automatically:

$$\begin{aligned}\langle\phi_{n'\mathbf{k}'}|\,\hat{\mathbf{p}}\,|\phi_{n\mathbf{k}}\rangle &= \hbar\Delta\mathbf{k}\delta_{\Delta\mathbf{k}'\Delta\mathbf{k}}\delta_{nn'} + \delta_{\Delta\mathbf{k}'\Delta\mathbf{k}}\langle\phi_{n'\mathbf{k}_0}|\,\hat{\mathbf{p}}\,|\phi_{n\mathbf{k}_0}\rangle \\ &= \langle\Delta\mathbf{k}'|\,\hat{\mathbf{p}}\,|\Delta\mathbf{k}\rangle\,\delta_{nn'} + \delta_{\Delta\mathbf{k}'\Delta\mathbf{k}}\langle\phi_{n'\mathbf{k}_0}|\,\hat{\mathbf{p}}\,|\phi_{n\mathbf{k}_0}\rangle \end{aligned} \tag{8}$$

Thus the matrix representation of momentum operator has the following form:

$$\hat{\mathbf{p}} \to \breve{\mathbf{p}} \otimes \widetilde{\mathbb{I}} + \breve{\mathbb{I}} \otimes \widetilde{\mathbf{p}} \tag{9}$$

where $\breve{O}$ denotes matrix representation of operator $\hat{O}$ in inner space, $\widetilde{O}$ denotes matrix representation in orbital space, $\breve{\mathbb{I}}$ is identity matrix in inner space, and $\widetilde{\mathbb{I}}$ is identity matrix in orbital space. As $\breve{O}$ acts only in the inner space and $\widetilde{O}$ acts only in the orbital space, we will neglect the identity matrix $\widetilde{\mathbb{I}}$ and $\breve{\mathbb{I}}$ in the rest of this paper.

For the vector potential, we divide it into a translation invariant part and a translation variant part:

$$\mathbf{A} = \mathbf{A}_i + \mathbf{A}_o \tag{10}$$

$$\mathbf{A}_i = \frac{1}{2}\mathbf{B} \times (\mathbf{r} - \mathbf{R})$$

$$\mathbf{A}_o = \frac{1}{2}\mathbf{B} \times \mathbf{R} \tag{11}$$

where $\mathbf{R}$ denotes the cell containing $\mathbf{r}$. $\mathbf{A}_i$ is the translation invariant part as shown in Fig. 2. It varies continuously in each unit cell and has steps on the boundaries of cells. It must be diagonal in orbital space because it do not carry any momentum:

$$\langle\phi_{n'\mathbf{k}'}|\,\mathbf{A}_i\,|\phi_{n\mathbf{k}}\rangle = \delta_{\Delta\mathbf{k}'\Delta\mathbf{k}}\langle\phi_{n'\mathbf{k}_0}|\,\mathbf{A}_i\,|\phi_{n\mathbf{k}_0}\rangle \tag{12}$$

Thus we denote the matrix form of $\mathbf{A}_i$ in inner space as $\breve{\mathbf{A}}$. $\mathbf{A}_o$ is the translation variant part as shown in Fig. 2. It keeps constant in each unit cell and has steps on the boundaries of cells. On the low energy scale, envelope functions vary so slowly that they nearly keep constant in each unit cell and hence non-zero fourier components of envelope functions satisfy $|\Delta\mathbf{k}\cdot\mathbf{a}_i| \ll 1$ with $\mathbf{a}_{i=123}$ are lattice vectors. Then we have the following statement:

$$\begin{aligned}\langle\phi_{n'\mathbf{k}'}|\,\mathbf{A}_o\,|\phi_{n\mathbf{k}}\rangle &= \sum_{\mathbf{R}}\int_{\text{cell}} d^3r\cdot\phi_{n'\mathbf{k}}(\mathbf{r}+\mathbf{R})\phi_{n\mathbf{k}}(\mathbf{r}+\mathbf{R}) \\ &\approx \delta_{n'n}\sum_{\mathbf{R}} e^{i(\Delta\mathbf{k}-\Delta\mathbf{k}')\cdot\mathbf{R}}\mathbf{A}_o(\mathbf{R}) \\ &\approx \delta_{n'n}\langle\Delta\mathbf{k}'|\,\mathbf{A}_o\,|\Delta\mathbf{k}\rangle \end{aligned} \tag{13}$$

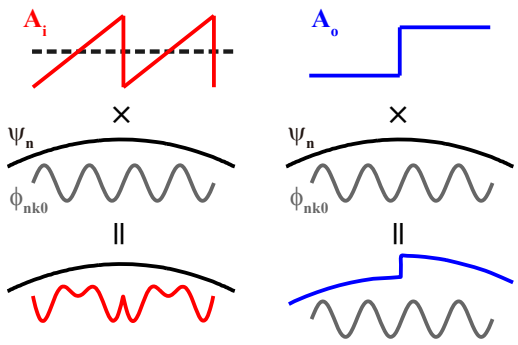

FIG. 2: Diagrammatic sketch of the divide of vector potential. The left part shows the translation invariant component $\mathbf{A}_i$ and how it acts on the Bloch wave functions $\phi_{n\mathbf{k}_0}$. The right part shows the translation variant component $\mathbf{A}_o$ and how it acts on the envelope functions ψ_n.

i.e. $\mathbf{A}_o$ is diagonal in inner space. Thus we denote the matrix representation of $\mathbf{A}_o$ in orbital space as $\widetilde{\mathbf{A}}$. Therefore we have successfully decomposed the vector potential into two operators act only in inner space or orbital space:

$$\mathbf{A} \to \breve{\mathbf{A}} + \widetilde{\mathbf{A}} \tag{14}$$

Scalar potential can also be easily decomposed. The crystal periodic potential acts only in inner space due to the same reason of $\mathbf{A}_i$ and we denote its operator matrix as $\breve{V}$. The external scaler field varies slowly hence we assume it can be expanded by $e^{i\Delta\mathbf{k}\cdot\mathbf{r}}$ with $\Delta\mathbf{k}$ in BZ. Thus the external field can not lead to inter-bands transition:

$$\begin{aligned}
\langle\phi_{n'\mathbf{k}'}|\, V\,|\phi_{n\mathbf{k}}\rangle &= \sum_{\Delta\mathbf{q}} V\left(\Delta\mathbf{q}\right)\langle\phi_{n'\mathbf{k}_0}|\, e^{i(\Delta\mathbf{k}+\Delta\mathbf{q}-\Delta\mathbf{k}')\cdot\mathbf{r}}\,|\phi_{n\mathbf{k}_0}\rangle \\
&= V\left(\Delta\mathbf{k}'-\Delta\mathbf{k}\right)\delta_{n'n} \\
&= \delta_{n'n}\langle\Delta\mathbf{k}'|\, V\,|\Delta\mathbf{k}\rangle
\end{aligned} \tag{15}$$

i.e. external scaler field acts only in orbital space. We denote the matrix form of V in orbital space as $\widetilde{V}$. Therefore the total scaler potential's matrix representation is:

$$V_0 + V \to \breve{V} + \widetilde{V} \tag{16}$$

B. Zeeman Effect

Using the direct product matrix form of operators (Eq. (9), Eq. (14) and Eq. (16)), we can go on to decompose the hamiltonian. We firstly rewrite the hamiltonian in Eq. (1) in a full matrix form:

$$H = \frac{\left(\breve{\mathbf{D}} + \widetilde{\mathbf{D}}\right)^2}{2m} + \breve{V} + \widetilde{V} + \mu_B \frac{g_0}{2} \breve{\boldsymbol{\sigma}} \cdot \mathbf{B} + \frac{\hbar}{4m^2c^2} \left(\breve{\mathbf{D}} + \widetilde{\mathbf{D}}\right) \cdot \breve{\boldsymbol{\sigma}} \times \nabla \breve{V} \tag{17}$$

in which $\breve{\mathbf{D}}$ and $\widetilde{\mathbf{D}}$ are defined as:

$$\breve{\mathbf{D}} = \breve{\mathbf{p}} + e\breve{\mathbf{A}} \tag{18}$$

$$\widetilde{\mathbf{D}} = \widetilde{\mathbf{p}} + e\widetilde{\mathbf{A}} \tag{19}$$

We note that Eq. (17) is the matrix representation of Eq. (1) on the bases we choose and hence all the operators in Eq. (1) have been replaced by matrices. For example, $\breve{\boldsymbol{\sigma}}$ are no longer pauli matrices but their representations:

$$\breve{\sigma}^i_{n'\mathbf{k}',n\mathbf{k}} = \langle \phi_{n'\mathbf{k}'} | \, \sigma^i \, | \phi_{n\mathbf{k}} \rangle \tag{20}$$

Then we divide Eq. (17) into several parts:

$$H = H_i + H_o + H_{io} + \mu_B \frac{g_0}{2} \breve{\boldsymbol{\sigma}} \cdot \mathbf{B} \tag{21}$$

$$H_i = \frac{\breve{\mathbf{D}}^2}{2m} + \breve{V} + \frac{\hbar}{4m^2c^2} \breve{\mathbf{D}} \cdot \breve{\boldsymbol{\sigma}} \times \nabla \breve{V} \tag{22}$$

$$H_o = \frac{\widetilde{\mathbf{D}}^2}{2m} + \widetilde{V} + \frac{\hbar}{4m^2c^2} \widetilde{\mathbf{D}} \cdot \breve{\boldsymbol{\sigma}} \times \nabla \breve{V} \tag{23}$$

$$H_{io} = \frac{\breve{\mathbf{D}} \cdot \widetilde{\mathbf{D}}}{m} \tag{24}$$

H_o describes a free electron with SOC in an external field $\widetilde{V}$. More than that, H_i concerns with inner space freedom and H_{io} describes the coupling between inner and orbital spaces. As the following investigation, a simple analogy to schrödinger equation of $\frac{1}{2}$-spin electron implies that H_i leads to Zeeman splitting, and H_{io} contributes to other SOC-like effects.

We firstly look at H_i, it can be expanded as:

$$H_i = \frac{\breve{\mathbf{p}}^2}{2m} + \breve{V} + \frac{\hbar}{4m^2c^2} \breve{\mathbf{p}} \cdot \breve{\boldsymbol{\sigma}} \times \nabla \breve{V} + \frac{e^2 \breve{\mathbf{A}}^2}{2m} + \frac{e}{m} \breve{\mathbf{A}} \cdot \breve{\boldsymbol{\pi}} \tag{25}$$

where $\boldsymbol{\pi} = \hat{\mathbf{p}} + \frac{\hbar}{4m^2c^2}\boldsymbol{\sigma} \times \nabla V$. The first line of Eq. (25) must be diagonal because it is just the hamiltonian of equilibrium crystal and we denote the diagonalized part as H_0. The most important effect comes from the last term of Eq. (25) which is the interaction between magnetic field and inner spaces. We reformulate it as:

$$\begin{aligned} \frac{e}{m}\breve{\mathbf{A}} \cdot \breve{\boldsymbol{\pi}} &= \frac{e}{2m}\mathbf{B} \times \breve{\mathbf{r}} \cdot \breve{\boldsymbol{\pi}} \\ &= \mu_B \frac{1}{\hbar}\breve{\mathbf{L}} \cdot \mathbf{B} \end{aligned} \tag{26}$$

$$\breve{\mathbf{L}} = \breve{\mathbf{r}} \times \breve{\boldsymbol{\pi}} \tag{27}$$

where $\breve{\mathbf{r}}$ is the matrix form of $\mathbf{r} - \mathbf{R}$ in inner space (it is diagonal in orbital space). This reveals that the extra Zeeman term has a origin of orbital angular momentum. Then H_i is reduced to:

$$H_i = H_0 + \frac{e^2\breve{\mathbf{A}}^2}{2m} + \mu_B \frac{1}{\hbar}\breve{\mathbf{L}} \cdot \mathbf{B} \tag{28}$$

We secondly sum up all the terms again:

$$\begin{aligned} H = H_0 + \frac{\widetilde{\mathbf{D}}^2}{2m} + \widetilde{V} + \frac{1}{m}\left(\breve{\boldsymbol{\pi}} + \breve{\mathbf{A}}\right) \cdot \widetilde{\mathbf{D}} + \frac{e^2\breve{\mathbf{A}}^2}{2m} \\ + \mu_B \left(\frac{1}{\hbar}\breve{\mathbf{L}} + \frac{g_0}{2}\boldsymbol{\sigma}\right) \cdot \mathbf{B} \end{aligned} \tag{29}$$

Finally we neglect second order quantities $\breve{\mathbf{A}} \cdot \widetilde{\mathbf{D}}$ and $\breve{\mathbf{A}}^2$, then the total hamiltonian is:

$$\begin{aligned} H = H_0 + \frac{\widetilde{\mathbf{D}}^2}{2m} + \widetilde{V} + \frac{1}{m}\breve{\boldsymbol{\pi}} \cdot \widetilde{\mathbf{D}} \\ + \mu_B \left(\frac{1}{\hbar}\breve{\mathbf{L}} + \frac{g_0}{2}\breve{\boldsymbol{\sigma}}\right) \cdot \mathbf{B} \end{aligned} \tag{30}$$

Apparently, the last term represents the Zeeman splitting and the last second term resembles the SOC term in schrödinger equation.

In systems with both inversion and time reversal symmetry, all states are at least double degenerate. If no further degeneration presents we can define the g-factor tensor as

$$B_i g_{ij} \tau_j = \left(2\frac{1}{\hbar}\breve{\mathbf{L}} + g_0\breve{\boldsymbol{\sigma}}\right) \cdot \mathbf{B} \tag{31}$$

where τ_j denote Pauli matrices for pseudo spin. In general, g-factor tensor has nigh independent components.[14,15] For free electron in vacuum, g-factor tensor is simply $2\delta_{ij}$. The observed g-factor by applying magnetic field along an unit vector $\mathbf{n}$ is indeed the eigenvalues of matrix $n_i g_{ij} \tau_j$ and can be calculated by $\sqrt{\sum_j (\sum_i n_i g^{ij})^2}$.

C. Computation

We use Vienna ab-initio simulation package (VASP) to compute $\breve{\mathbf{L}}$ and $\breve{\boldsymbol{\sigma}}$ in a first principles way. VASP uses a standard projected augmentation wave function (PAW)[16,17] data in which any operator matrix element can be calculated by:

$$\begin{aligned}\langle\varphi'|O|\varphi\rangle &= \langle\widetilde{\varphi}'|O|\widetilde{\varphi}\rangle \\ &+ \sum_{ij}\langle\widetilde{\varphi}'|\widetilde{p}_i\rangle\big(\langle\phi_i|O|\phi_j\rangle - \langle\widetilde{\phi}_i|O|\widetilde{\phi}_j\rangle\big)\langle\widetilde{p}_j|\widetilde{\varphi}\rangle\end{aligned} \tag{32}$$

where $\widetilde{\varphi}$ is the pseudo (PS) wave function stored in plane-waves, φ is corresponding all-electron (AE) wave function, $\widetilde{p}_i$ is projector function, $\widetilde{\phi}_i$ is PS partial wave, ϕ_i is AE partial wave. Calculation of $\breve{\boldsymbol{\sigma}}$ is very easy to actualize. What we need to do is just replacing O in Eq. (32) with pauli matrices and all the needed subroutines to calculate terms in Eq. (32) are available in VASP source code. While calculation of $\breve{\mathbf{L}}$ is a little more complicated. Our strategy is to calculate $\breve{\mathbf{r}}$ and $\breve{\boldsymbol{\pi}}$ respectively and then calculate their cross product. It is very convenient to calculate $\breve{\boldsymbol{\pi}}$ in the PAW frame work. We add some codes in VASP to compute $\breve{\mathbf{p}}$ and $\boldsymbol{\sigma}\times\nabla\breve{V}$ individually and add them together in the end. We note that we keep the approximation of VASP that $\nabla\breve{V}$ is taken into account only in the augmentation region, which is good enough because the potential outside varies much more slowly than the potential inside. However, there is no direct method to calculate $\breve{\mathbf{r}}$ in the PAW framework. But thanks to the commutation relation $[\breve{\mathbf{r}}, H_0] = \frac{i\hbar}{m}\breve{\boldsymbol{\pi}}$, we can calculate it by the following relation :

$$(E_n - E_l)\,\breve{\mathbf{r}}_{nl} = -i\frac{\hbar}{m}\breve{\boldsymbol{\pi}}_{nl} \tag{33}$$

But it still seems to be problematic for the terms with $E_n = E_l$. Let us notice that in centrosymmetric systems degenerate states at $\mathbf{k}_0$ (chosen to be inversion invariant momenta (IIM)) usually possess the same parity. In this case $\breve{\mathbf{r}}$ elements between these degenerate states should vanish due to parity conservation. We will return to the applicable conditions later and assume $E_n \neq E_l$ for now:

$$\breve{\mathbf{L}}_{nm} = -\frac{i\hbar}{m}{\sum_{l}}' \frac{\breve{\boldsymbol{\pi}}_{nl}\times\breve{\boldsymbol{\pi}}_{lm}}{E_n - E_l} \tag{34}$$

where the summation over l only takes the cases that $\phi_{l\mathbf{k}_0}$ has different parity with $\phi_{n\mathbf{k}_0}$ and $\phi_{m\mathbf{k}_0}$.

TABLE I: Computed and Experimental g-factor tensors. All g-factor tensors are calculated using the experimental structure[19,20]. Definitions of g-factor tensors can be found in the text. Gap here means the direct gap at the bands top or bottom.

Method	Bi-h			Bi-e					Bi_2Se_3-e		
	gap (eV)	$g_\perp$	$g_\parallel$	gap (eV)	g_{11}	g_{22}	g_{32}	g_{33}	gap (eV)	$g_\perp$	$g_\parallel$
LDA	0.272	0	78.5	0.113	-11.1	137	10.7	-11.5	0.521	16.5	18.4
GGA	0.298	0	73.8	0.102	-11.8	152	12.0	-12.3	0.435	17.9	21.7
LDA+mBJ	0.453	0	55.3	-0.002	*	*	*	*	0.236	26.2	41.8
HSE06	0.493	0	50.9	0.0069	137	2188	190	168	0.250	26.2	37.4
EXP	0.18-0.41[21]	0	63.2[22]	0.011-0.015[21]						23[23]	32[23]

Now we investigate the applicable conditions carefully. We should notice that for all crystal point groups with inversion symmetry, each irreducible representation (IR) has a determined parity[18]. Therefore, for symmorphic space group any necessary degenerate states at IIMs have the same parity, because the little groups at these IIMs are just some centrosymmetric point groups and the IRs at IIMs is equivalent to the point groups' IRs. However, the argument can not hold for non-symmorphic space groups. For a non-symmorphic space group, IRs at Γ is still equivalent with IRs of a centrosymmertic point group (little group at Γ) which are called relevant representations, while IRs at other IIMs on BZ boundaries are in general not equivalent with point group's IRs due to additional degeneration. In the latter case, degenerates states may possess different parities. Therefore our computation formula can be applied for general IIMs in centrosymmetric systems with symmorphic space groups and Γ in centrosymmetric systems with non-symmorphic space groups.

III. MATERIALS

In this section, we apply our method to calculate g-factor tensors of bismuth and Bi_2Se_3. Both of them have centrosymmetric and symmorphic space group, for which our method is applicable. Exchange and correlation (XC) potential is treated within some most widely used types : the Perdew-Zunger[24] (PZ) type local density approximation (LDA) , Perdew-Burke-Ernzerhof[25] (PBE) type generalized gradient approximation (GGA), LDA correlation +

modified Becke and Johnson (mBJ) exchange[26] potential, and Heyd-Scuseria-Ernzerhof[27,28] (HSE) type hybrid functionals. Our numerical results are summarized in table I, which shows strong dependence of g-factors on XC potentials. The reason of this dependence is that the largest contributions to the g-factor are inversely proportional to the gap (Eq. (34)) which depends on XC potentials strongly. Thus functionals that give more accurate gaps will also give more accurate g-factors. That's why we apply LDA+mBJ and HSE calculations, which are believed to be better than LDA or GGA in predicting gaps. To calculate Eq. (34), we must choose a bands cutoff for the matrix multiplication. After some test of convergence, we find 120 bands are enough to capture the most contributions.

A. Bismuth

Bismuth is a semi-metal with one hole pocket at T(001) and three electron pockets at L.[21] It has a symmorphic space group $R\bar{3}m$, which consist of a three folds z axis, a two folds x axis and an inversion operation. There has been a lot of interest in its large and anisotropic g-factors[10–12,22]. In the followings, we firstly perform symmetry analysis and then show first principles calculations results.

Let us begin with the holes. T point , where the hole pocket locates, possesses little group D_{3d}. We calculate the characters of wave functions and find that hole bands carry IRs ${}^1E_{3/2,u}$ and ${}^2E_{3/2,u}$ (transform as $|P_{\frac{3}{2}}, \frac{3}{2}\rangle$ and $|P_{\frac{3}{2}}, \frac{\bar{3}}{2}\rangle$) which are degenerate due to time reversal symmetry.[18] As the principle axis is three folds, only the module by 3 of angular momentum makes sense. Thus $|P_{\frac{3}{2}}, \frac{3}{2}\rangle$ and $|P_{\frac{3}{2}}, \frac{\bar{3}}{2}\rangle$ transform equivalently under C_3, and due to angular moment conservation there must be $\breve{\sigma}_\pm = \breve{\sigma}_x \pm i\breve{\sigma}_y = 0$, $\breve{L}_\pm = \breve{L}_x \pm i\breve{L}_y = 0$ and $\breve{\sigma}_z/\breve{L}_z$ are some hermitian matrices. Therefore the anisotropy has a pure symmetry origin. We can use a unitary transform to diagonalize $\sigma_z + \frac{1}{\hbar}\breve{L}_z$ and then the g-factor tensor takes the form:

$$g_h = \begin{pmatrix} 0 & 0 & 0 \\ 0 & 0 & 0 \\ 0 & 0 & g_\parallel \end{pmatrix} \tag{35}$$

Secondly, we investigate the electrons. For simplicity, let us focus on the electron pocket locates in the y-z plane (L_1). Little group of L_1 is C_{2h} which contains a two folds x-axis and an inversion operation. Electron bands at L_1 carry IRs ${}^1E_{\frac{1}{2},g}$ and ${}^2E_{\frac{1}{2},g}$ (transform as $|S_{\frac{1}{2}}\frac{1}{2}\rangle$

and $|S_{\frac{1}{2}}\bar{\frac{1}{2}}\rangle$) which are degenerate due to time reversal symmetry.[18] Under the symmetry condition, spin and orbital angular momentum should take the form:

$$\sigma_x + \frac{1}{\hbar}\breve{L}_x \propto \tau_x \tag{36}$$

$$\sigma_y + \frac{1}{\hbar}\breve{L}_y \propto \tau_y \text{ mix } \tau_z \tag{37}$$

$$\sigma_z + \frac{1}{\hbar}\breve{L}_z \propto \tau_y \text{ mix } \tau_z \tag{38}$$

While we still have a gauge freedom $e^{-i\alpha\tau_x/2}$ to choose $\sigma_y + \frac{1}{\hbar}\breve{L}_y$ proportional to τ_y. In this gauge the g-factor tensor takes the form:

$$g_e = \begin{pmatrix} g_{11} & 0 & 0 \\ 0 & g_{22} & 0 \\ 0 & g_{32} & g_{33} \end{pmatrix} \tag{39}$$

Both T and L can be thought as gapped (by (SOC)) Dirac points. Thus the main contribution to g-factors are proportional to $\frac{v^2}{\Delta}$ due to Eq. (34), where v is Dirac velocity and Δ is gap. Therefore the large value of g-factors can be ascribed to large Dirac velocities or small gaps. Different XC potentials give similar v but very different Δ. At T point, LDA+mBJ gives the gap and g-factor closest to experimental data. However gap at L calculated by LDA+mBJ are slightly closed: $E_{\frac{1}{2},g}$ bands are moved below $E_{\frac{1}{2},u}$ bands about 2 meV. The experimental gap at L is indeed very small (0.011-0.015eV[21]), therefore we can expect huge g-factors for electrons.

B. Bi_2Se_3-electrons

Bi_2Se_3 has been a famous material in the past few years as the first large gap ($\sim$0.3eV) three dimensional $\mathbb{Z}_2$ topological insulator.[29–31] Besides its non trivial topology, Bi_2Se_3 also has non trivial large g-factors (32 along z-axis and 23 in x-y plane).[23] It also possesses the symmetry of $R\bar{3}m$. By calculating characters, we find the conduction bands at Γ are bases of IR $E_{1/2,u}$ and transform as $|P_{\frac{1}{2}}, \frac{1}{2}\rangle$ and $|P_{\frac{1}{2}}, \bar{\frac{1}{2}}\rangle$.[18] Due to angular momentum conservation, there should be non zero $\sigma_\pm + \frac{1}{\hbar}\breve{L}_\pm$ and $\sigma_z + \frac{1}{\hbar}\breve{L}_z$, and they have the form:

$$\sigma_{x/y} + \frac{1}{\hbar}\breve{L}_{x/y} = \frac{1}{2}g_\perp \cdot \tau_{x/y} \tag{40}$$

$$\sigma_z + \frac{1}{\hbar}\breve{L}_z = \frac{1}{2} g_{\parallel} \cdot \tau_z \tag{41}$$

Therefore g-factor tensor takes the form:

$$g_e = \begin{pmatrix} g_\perp & 0 & 0 \\ 0 & g_\perp & 0 \\ 0 & 0 & g_{\parallel} \end{pmatrix} \tag{42}$$

As shown in tabel.I, Bi_2Se_3 has a large gap at Γ. Thus the large g-factors should be ascribed to the large Dirac velocity, which may be a result of bands inversion.

Because maximum points of valence bands are not Γ but some points a little deviated from it, gap measured by experiments is the indirect gap. Thus we can not compare our calculated direct gaps with experimental data. But we think LDA and GGA overestimate the gap hence underestimate the g-factors, while LDA+mBJ and HSE underestimate the gap hence overestimate the g-factors.

IV. CONCLUSION

Due to translational symmetry, the Hilbert space is decomposed as direct product of orbital space and inner space. In this point of view, Zeeman splitting can be interpreted as the interaction between inner space and magnetic field. Depend on this understanding, a first principles computation method of g-factors has been developed. Our method successfully gives comparable g-factors with experimental data for bismuth and B_2Se_3. Specifically, our analysis reveals that the anisotropy in bismuth is a consequence of symmetry and the large values of g-factors in bismuth and Bi_2Se_3 can be ascribed to the large Dirac velocities or small gaps. On the other hand, our method is limited for centrosymmetric systems. In systems with symmorphic space group bases should be chosen at IIMs, while in systems with non-symmorphic space group bases can only be chosen at Γ in general. Thus both further development of this method and calculating more materials are strongly recommended.

ACKNOWLEDGMENTS

This work was supported by the National Natural Science Foundation of China, the 973 program of China (No.2013CB921700), and the "Strategic Priority Research Program (B)"

of the Chinese Academy of Sciences (No.XDB07020100).

---

* daix@iphy.ac.cn

[1] J. M. Luttinger, Physical Review **102**, 1030 (1956).

[2] M. H. Cohen and E. I. Blount, Philosophical Magazine **5**, 115 (1960).

[3] M.-C. Chang and Q. Niu, Physical Review B **53**, 7010 (1996).

[4] M.-C. Chang and Q. Niu, Journal of Physics: Condensed Matter **20**, 193202 (2008).

[5] D. Vanderbilt and R. D. King-Smith, Physical Review B **48**, 4442 (1993).

[6] R. D. King-Smith and D. Vanderbilt, Physical Review B **47**, 1651 (1993).

[7] R. Resta, Reviews of Modern Physics **66**, 899 (1994).

[8] D. Xiao, M.-C. Chang, and Q. Niu, Reviews of Modern Physics **82**, 1959 (2010).

[9] T. Thonhauser, International Journal of Modern Physics B **25**, 1429 (2011).

[10] G. E. Smith, G. A. Baraff, and J. M. Rowell, Physical Review **135**, A1118 (1964).

[11] V. S. del'man, Soviet Physics Uspekhi **20**, 819 (1977).

[12] J. Alicea and L. Balents, Physical Review B **79**, 241101 (2009).

[13] J. M. Luttinger and W. Kohn, Physical Review **97**, 869 (1955).

[14] E. Ivchenko, A. Kiselev, and M. Willander, Solid state communications **102**, 375 (1997).

[15] A. Kiselev, E. Ivchenko, and U. Rössler, Physical Review B **58**, 16353 (1998).

[16] P. E. Blchl, Physical Review B **50**, 17953 (1994).

[17] G. Kresse and D. Joubert, Physical Review B **59**, 1758 (1999).

[18] S. L. Altmann and P. Herzig, *Point-group theory tables* (Clarendon Press, 1994).

[19] C. Barrett, Australian Journal of Physics **13**, 209 (1960).

[20] S. Nakajima, Journal of Physics and Chemistry of Solids **24**, 479 (1963).

[21] Y. Liu and R. E. Allen, Physical Review B **52**, 1566 (1995).

[22] H. R. Verdn and H. D. Drew, Physical Review B **14**, 1370 (1976).

[23] H. Khler and E. Wchner, physica status solidi (b) **67**, 665 (1975).

[24] J. P. Perdew and A. Zunger, Physical Review B **23**, 5048 (1981).

[25] J. P. Perdew, K. Burke, and M. Ernzerhof, Physical Review Letters **77**, 3865 (1996).

[26] F. Tran and P. Blaha, Physical Review Letters **102**, 226401 (2009).

[27] J. Heyd, G. E. Scuseria, and M. Ernzerhof, The Journal of Chemical Physics **118**, 8207 (2003).

[28] J. Heyd, G. E. Scuseria, and M. Ernzerhof, The Journal of Chemical Physics **124**, 219906 (2006).

[29] H. Zhang, C.-X. Liu, X.-L. Qi, X. Dai, Z. Fang, and S.-C. Zhang, Nature Physics **5**, 438 (2009).

[30] Y. Zhang, K. He, C.-Z. Chang, C.-L. Song, L.-L. Wang, X. Chen, J.-F. Jia, Z. Fang, X. Dai, W.-Y. Shan, S.-Q. Shen, Q. Niu, X.-L. Qi, S.-C. Zhang, X.-C. Ma, and Q.-K. Xue, Nature Physics **6**, 584 (2010).

[31] C.-X. Liu, X.-L. Qi, H. Zhang, X. Dai, Z. Fang, and S.-C. Zhang, Phys. Rev. B **82**, 045122 (2010).